ACS APPLIED MATERIALS & INTERFACES

Research Article

www.acsami.org

High-Performance Triethylsilylethynyl Anthradithiophene Transistors Prepared without Solvent Vapor Annealing: The Effects of Self-Assembly during Dip-Coating

Sooji Nam,[†,▽] Jaeyoung Jang,[†,▽] John. E. Anthony,[§] Jong-Jin Park,*[,‡] Chan Eon Park,*[,†] and Kinam Kim[‡]

[†]Postech Organic Electronics Laboratory, Polymer Research Institute, Department of Chemical Engineering, Pohang University of Science and Technology (POSTECH), Pohang, 790-784, Republic of Korea

[‡]Samsung Advanced Institute of Technology (SAIT), Yongin, 449-712, Republic of Korea

[§]Department of Chemistry, University of Kentucky, Lexington, Kentucky, 40506, United States

Supporting Information

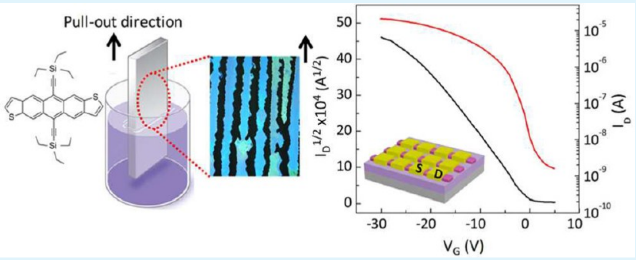

ABSTRACT: Solution-processable small-molecule organic semiconductors have recently attracted significant attention for use as the active channel layers in organic field-effect transistors due to their good intrinsic charge carrier mobility and easy processability. Dip-coating is a good method for optimizing the film morphology and molecular ordering of the small-molecular semiconductors because the drying speed can be quantitatively controlled at the air−solution−substrate contact line. Here, we report the preparation of highly crystalline triethylsilylethynyl−anthradithiophene (TES-ADT) crystal arrays that exhibit an excellent field-effect mobility (up to 1.8 cm^2/(V s)) via an optimized one-step dip-coating process. High-quality TES-ADT crystals were grown without solvent vapor annealing postprocessing steps, which were previously thought to be essential for improving the morphology, crystallinity, and electrical characteristics of TES-ADT thin films. An interesting correlation between the optimal pull-out rate and the self-assembly tendencies of some soluble acene semiconductors was observed, and the origin of the correlation was investigated. Our work demonstrates an alternative simple approach to achieving highly crystalline TES-ADT thin films, and further proposes a prospective method for optimizing the formation of thin films via the molecular self-assembly of soluble acenes.

KEYWORDS: *soluble acenes, evaporation-induced self-assembly, without solvent-vapor annealing, solution-process, dip-coating, organic field-effect transistors*

■ INTRODUCTION

Organic semiconducting materials have recently attracted significant attention for use as active channel layers in organic field-effect transistors (OFETs) due to their mechanical flexibility and low-cost, simple, and low-temperature processability.[1−3] Organic small molecules with solublizing side groups are especially promising materials because they have good intrinsic charge carrier mobilities while maintaining the advantages of solution processability by means of spin-coating, drop-casting, inkjet-printing, or dip-coating.[4−7] Although small molecule semiconductors can be readily solution-deposited, their film morphologies and crystallinities are sensitive to the processing conditions, including the solvent, deposition method, and postannealing processing steps.[8−10] Because the molecular ordering or packing states in active layers are crucial for determining the performances of OFETs, many research groups have endeavored to enhance OFET performances by controlling these processing conditions.[11−13] The preparation of highly crystalline organic semiconductor thin films with high field-effect mobilities (exceeding 1.0 cm^2/(V s)) via a simple and reproducible approach remains a challenge.

Triethylsilylethynyl−anthradithiophene (TES-ADT), a representative functionalized soluble acene material, can potentially yield excellent electrical characteristics due to its good crystallinity and large grain size obtained after solvent vapor annealing procedures. The as-spun TES-ADT films generally display a low crystallinity and poor OFET performances (with mobilities below 0.01 cm^2/(V s)), solvent vapor annealing is thought to be an essential processing step, providing the only method for improving the crystallinity and performance of TES-ADT thin films;[14−16] however, solvent vapor annealing procedures do not guarantee uniformity over the entire film surface, and they may complicate device fabrication processes. Nevertheless, alternative approaches to improving the crystal-

Received: December 20, 2012
Accepted: March 5, 2013
Published: March 5, 2013

dx.doi.org/10.1021/am303192b | *ACS Appl. Mater. Interfaces* 2013, 5, 2146−2154

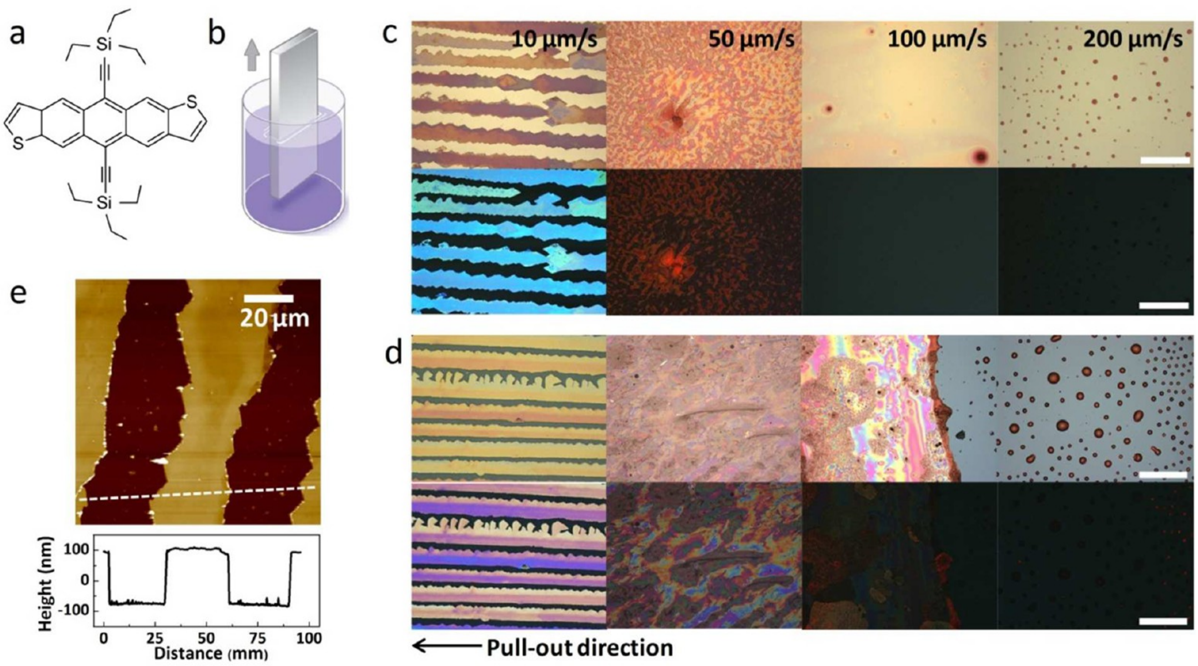

Figure 1. (a) Chemical structure of TES-ADT used in this study. (b) Simplified schematic illustration of the dip-coating process. OM and POM images of the dip-coated TES-ADT thin films formed on (c) Al_2O_3 or (d) SiO_2 dielectrics, respectively (all scale bars indicate 100 μm). (e) Noncontact mode AFM topograph and height profile of TES-ADT crystals grown at 10 μm/s. The AFM image and height profile indicate a uniform thickness of 195 ± 10 nm and an interval of 25 μm for three adjacent crystals.

linity and electrical characteristics of TES-ADT thin films are scarce. Lee et al.[15] reported a processing method for controlling the grain size of TES-ADT thin films. The addition of a small quantity of fluorinated 5,11-bis(triethylsilylethynyl) anthradithiophene (FTES-ADT) to the TES-ADT solution seeded crystallization in the resulting spin-coated films via solvent vapor annealing. One recent study demonstrated the fabrication of highly crystalline TES-ADT thin films without any postdeposition processing at low casting temperature (below glass transition temperature of TES-ADT).[17] Although these strategies showed promise for increasing the crystallinity in the TES-ADT films, the typical device performance of resulting devices was not superior to that of the optimized TES-ADT devices with general solvent vapor annealing processes,[18,19] which suggests the possibility of further improving device performance.

In our previous study, we introduced a facile one-step approach to growing self-aligned highly crystalline FTES-ADT and 6,13-bis(triisopropylsilylethynyl) pentacene (TIPS-PEN) crystal arrays via an optimized dip-coating process.[20] We found that the optimized acene crystals could be grown at a specific pull-out rate (not too fast nor too slow), depending on the solvent evaporation rate at the contact line. Uniaxially oriented organic semiconductor crystals are desirable for achieving a high charge carrier mobility in OFET applications due to a high crystallinity and low crystalline mismatch along the charge transport direction.[7,11,21,22] In the present study, a facile one-step dip-coating process was used to demonstrate the preparation of highly crystalline TES-ADT crystal arrays showing excellent field-effect mobility values (up to 1.8 $cm^2/(V\ s)$) without the need for solvent vapor annealing. Contrasting with the results of our previous study using FTES-ADT and TIPS-PEN, high-quality TES-ADT crystal arrays were achieved at relatively slow pull-out rates during a dip-coating process. We propose a possible reason based on the investigation of the degree of self-organization in each of three soluble acene materials. Our findings provide a simple and reproducible method for creating highly crystalline TES-ADT crystals and suggest a facile route to the optimization of films formed from a variety of soluble acenes having different self-assembly tendencies.

■ EXPERIMENTAL SECTION

Materials and Sample Preparation. For OFET devices fabrication, heavily doped *n*-type Si wafers were used as substrates and gate electrodes. An Al_2O_3 gate dielectric layer, 100 nm thick, was deposited on the substrate by atomic layer deposition (ALD). A thermally grown 100 nm thick SiO_2 was also used as the gate dielectric. The substrate was dipped into a TES-ADT (synthesized by Anthony and co-workers[23]) solution (0.7 wt % in dichloromethane) at a constant rate of 1000 μm/s, then was lifted out at a constant rate of 10, 50, 100, or 200 μm/s. Dip-coating was performed in an acrylic box on a shock-absorbing optical table to reduce the effects of air currents, mechanical vibrations, and noise. After a few times (7−10) of dip-coatings, 1−2 drops of solvent was added to the vial to maintain the surface level of the solution. Gold source (S)/drain (D) electrodes were deposited by thermal evaporation through a shadow mask on the active layer. Each of the resulting square gold patterns had a 55.0 μm width, and the interval between patterns was 22.5 μm. To accurately determine the crystal field-effect mobility (μ), the channel width (W) values of individual crystals were determined independently from the optical microscopy image, and then, the W values were applied to calculate the crystal mobility values.

Characterization. Crystal thickness was determined using a surface profiler (Alpha-step 500, KLA Tencor). The optical microscopy (OM) and polarized optical microscopy (POM) images were obtained using an optical microscope (OLS 3000, Olympus). All POM images were recorded under cross-polarization with a constant polarizer angle. High-resolution out-of-plane X-ray diffraction (XRD) experiments were performed at the 10C1 beamline (λ = 1.54 Å) at the Pohang Accelerator Laboratory, Pohang, Korea. Atomic force

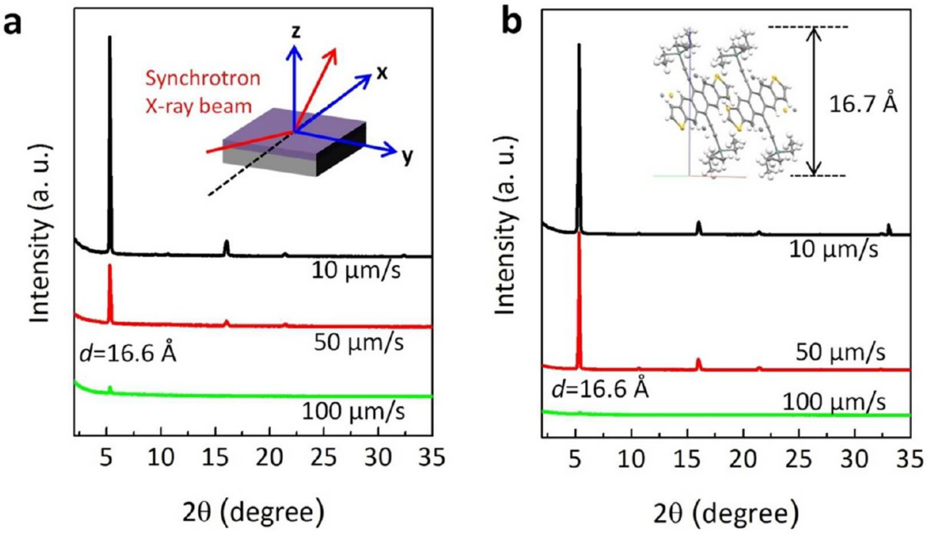

Figure 2. High-resolution θ−2θ mode out-of-plane XRD patterns of the TES-ADT thin films on (a) Al_2O_3 and (b) SiO_2 dielectrics, respectively. (a inset) Schematic illustration of the XRD experiment. (b inset) Crystallographic packing pattern and molecular axes of the TES-ADT molecules.

microscopy (AFM) images were collected using an atomic force microscope (Digital Instrument Multimode SPM). Two-dimensional grazing incidence wide-angle XRD (2D-GIXD) experiments were performed at the 4C2 beamline (wavelength = 1.38 Å) at the Pohang Accelerator Laboratory in Korea. The incidence angle of the X-ray beam was set to 0.16°. Samples were mounted on a home-built *z*-axis goniometer equipped with a vacuum chamber, and data were typically collected using a two-dimensional charge-coupled detector (2D CCD: Roper Scientific, Trenton, NJ, USA). All I−V characteristics of the devices and capacitances per unit area (C_i) of the gate dielectrics were measured in ambient air (relative humidity, 45 ± 15%) using a source/measurement unit (Keithley 4200) and a 4284 precision LCR meter (Agilent Tech), respectively. The mean C_i values of the 100 nm thick Al_2O_3 and SiO_2 gate dielectrics were found to be, respectively, 64 and 32.4 nF/cm^2. The field-effect mobility of each acene crystal was calculated from the transfer curves in the saturation regime, swept over the V_G range +5 to −20 V for OFETs on the Al_2O_3 gate dielectric, and +5 to −30 V for OFETs on the SiO_2 gate dielectric, using the equation, $ID = \mu C_i W(2L)^{-1}(V_G - V_{Th})^2$ where V_{Th} is the threshold voltage. A total of 18−32 FETs (6−8 FETs in a batch, 3−4 batches in total) were tested, and the FET parameters were averaged. For in situ time-resolved confocal microscopy (OLS 3000, Olympus) analysis, solutions of TES-ADT, TIPS-PEN, and FTES-ADT in toluene (0.2 wt %) were prepared, and 10 μL droplets were dropped onto the cleaned Si wafers. UV−vis (Cary, Varian Co.) measurements were used to analyze the optical properties of the active layers.

■ RESULTS AND DISCUSSION

Characterization of the TES-ADT Crystal Arrays. Figure 1a shows the chemical structure of TES-ADT used in this study, and Figure 1b illustrates a schematic representation of the dip-coating process. TES-ADT was dissolved in dichloromethane to form a 0.2 wt % solution. Two types of substrate (with 100 nm thick Al_2O_3 or SiO_2 dielectric layer surfaces) were used for the dip-coating experiment to confirm the pull-out rate-dependent crystallization behavior of TES-ADT on different types of substrate. Although both substrates show very flat and smooth surface characteristics, they have different surface chemical structure and dielectric constants. Like the SiO_2 layers, which are the most popular gate dielectrics of thin-film transistors, the Al_2O_3 layers (anodized or deposited by ALD) are also frequently used not only in the OFETs but also in the inorganic transistors based on graphene or oxide semiconductors.[24−26] Each substrate was dipped into the TES-ADT solution and pulled out at a constant rate of 10, 50, 100, or 200 μm/s. Figures 1c and d show OM and POM images of the dip-coated TES-ADT crystals formed on the Al_2O_3 and SiO_2 substrates, respectively. The TES-ADT molecules crystallized into continuous stripes on both substrates during the 10 μm/s upward pull-out step. Consistent brightness and color in the POM images indicated the presence of uniform and ordered crystalline structures of the TES-ADT crystal arrays.[27] The noncontact mode atomic force microscopy (AFM) topographs of three adjacent crystals and their height profiles, shown in Figure 1e, indicated a uniform thickness of 195 ± 10 nm and an interval of 25 μm. Films produced at a pull-out rate of 50 μm/s displayed a variety of film morphologies, mainly partially formed spherulite grains (see the Supporting Information Figure S1 for an illustration of the various film morphologies). The film morphologies were similar to those of spin-coated TES-ADT films prepared with solvent vapor annealing.[14,16] Although parts of the dip-coated TES-ADT films formed with a pull-out rate of 50 μm/s showed good crystalline morphologies in the POM images, the grain size was not uniform and did not cover the entire coated area. At faster pull-out rates (100 μm/s), the TES-ADT films showed featureless morphologies over large areas with poor crystallinities. The films eventually dewetted from both the Al_2O_3 and SiO_2 substrates at pull-out rates above 100 μm/s, probably due to insufficient time for film formation, in agreement with a recent report by Li et al.[28]

The crystallinities of TES-ADT films produced at different pull-out rates were characterized via θ−2θ mode out-of-plane XRD analysis conducted using a high-resolution synchrotron X-ray source. Figure 2a and b shows, respectively, the specular diffraction patterns of TES-ADT films with various substrate pull-out rates, formed on Al_2O_3 and SiO_2 substrates. All diffraction patterns consisted of [00l] peaks corresponding to a *d*-spacing of 16.6 Å, obtained from Bragg's law, $2d \sin\theta = n\lambda$. The *d*-spacing values of the TES-ADT films matched the reported *c*-axis length, 16.7 Å (see the molecular axes of TES-ADT in the inset of Figure 2b), indicating that the TES-ADT molecules stacked with silyl groups on the substrates.[10,21] The crystals grown under a pull-out rate of 10 μm/s showed the

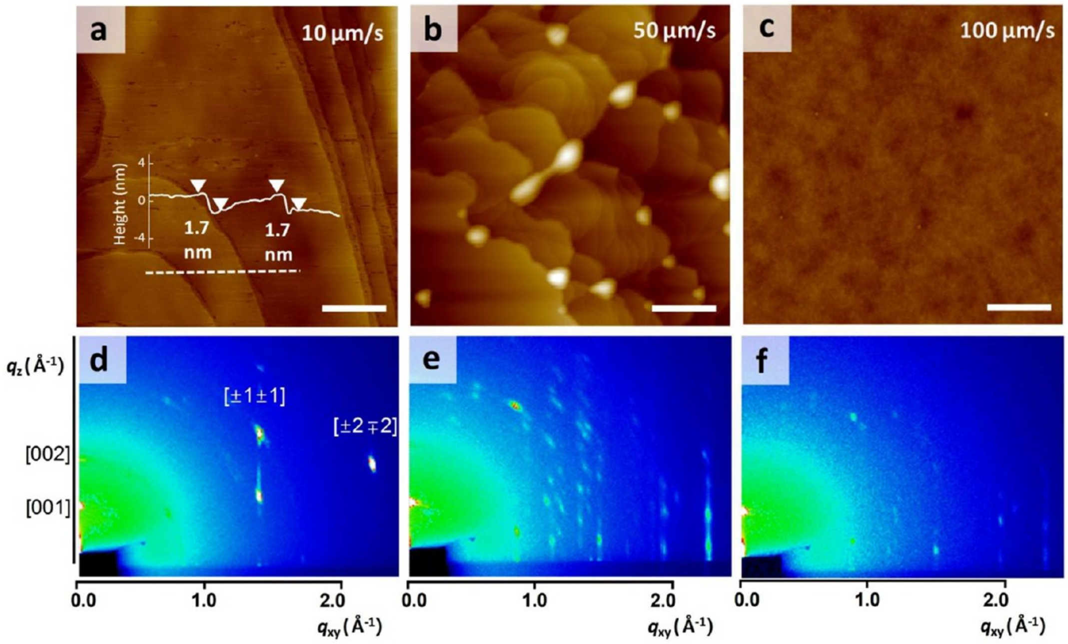

Figure 3. AFM topographs of the TES-ADT thin films produced at different pull-out rates: (a) 10, (b) 50, and (c) 100 μm/s, respectively (all scale bars indicate 1 μm). 2D-GIXD patterns of the TES-ADT thin films produced at (d) 10, (e) 50, and (f) 100 μm/s, respectively.

highest [00l] peak intensities among the films prepared on both substrates, suggesting that the crystal arrays produced at 10 μm/s pull-out rates yielded the highest crystallinities along the out-of-plane direction. In out-of-plane XRD, the peak intensities are generally proportional to the film thickness as well as the crystallinity.[29,30] Because the thicknesses of the films produced at pull-out rates of 10 or 50 μm/s were comparable (about 200 nm), the effects of the film thickness variations on the XRD peak intensities appeared to be negligible. Figures 3a−c show representative AFM topographs of the TES-ADT films produced at different pull-out rates of 10, 50, and 100 μm/s, respectively. As illustrated in the images, the TES-ADT crystals grown at 10 μm/s displayed large flat terrace surface morphologies. The heights of each tile (17 Å) coincided with the length of the *c*-axis in the TES-ADT crystals (16.7 Å).[23] On the other hand, crystals grown at 50 μm/s revealed many irregular steps and valleys in the small polycrystalline domains, and the film grown at 100 μm/s showed a nearly amorphous morphology. The AFM analysis clearly supported the out-of-plane mode XRD results.

The relationship between the pull-out rate and the molecular ordering was further examined by analyzing the crystalline structures of the TES-ADT thin films using 2D-GIXD techniques with a fixed grazing incidence angle of 0.16°. The incident beam direction was perpendicular to the sample dip-coating pull-out direction (see the Supporting Information Figure S2, which shows a schematic illustration of the 2D-GIXD experiment for dip-coated TES-ADT thin films). As illustrated in Figure 3f, the number of reflection spots in the TES-ADT films formed at pull-out rates of 100 μm/s was small, and their intensities were very weak, implying a low crystallinity along the in-plane direction, as in the case of the out-of-plane direction. Compared to these films, the number of reflection spots in the TES-ADT films formed at a pull-out rate of 50 μm/s increased along the q_z (out-of-plane) and q_{xy} (in-plane) directions, and the peak intensities were slightly strengthened (see Figure 3e). These results indicated that the TES-ADT thin films included many crystal domains with different crystalline orientations, corresponding to the surface morphologies shown in the AFM topographs. The 2D-GIXD patterns were similar to those of the spin-coated TES-ADT films reported previously, including spin-coated TES-ADT films before (corresponding to the dip-coated films prepared with a pull-out rate of 100 μm/s) and after (corresponding to the dip-coated films prepared with a pull-out rate of 50 μm/s) solvent vapor annealing.[10,19,31] The number of reflection spots for the TES-ADT crystal arrays grown at a pull-out rate of 10 μm/s was significantly reduced, but the peak intensities remarkably increased, as illustrated in Figure 3d. This 2D-GIXD pattern suggested that the crystalline orientations were simplified and the crystalline nanostructures became more ordered and dense in the aligned TES-ADT crystal arrays compared to the films obtained at higher pull-out rates. In other words, the π−π interactions among the TES-ADT molecules along the charge transport (in-plane) direction were maximized. A distribution of crystal orientations along the charge transport direction in an active layer is disadvantageous for charge carrier transport and achieving high OFET performances due to a large degree of crystalline mismatch along the charge transport direction.

The OFET performances of the TES-ADT thin films were investigated by fabricating top-contact OFETs with Au S/D electrodes. Figure 4a illustrates the fabrication processes and schematic device structures of OFETs. As shown in the schematic diagrams and OM images in the Supporting Information Figure 4a, individual crystals were characterized separately to accurately determine the crystal field-effect mobility for crystals grown at a pull-out rate of 10 μm/s. Figure 4b and c show the typical drain current (I_D) versus gate voltage (V_G) transfer characteristics and $I_D^{1/2}$ versus V_G characteristics for TES-ADT films and crystals grown at different lifting rates on the Al_2O_3 and SiO_2 substrates, respectively. As expected, the crystals grown at 10 μm/s exhibited superior field-effect mobilities that were orders of magnitude greater than those measured in thin films obtained

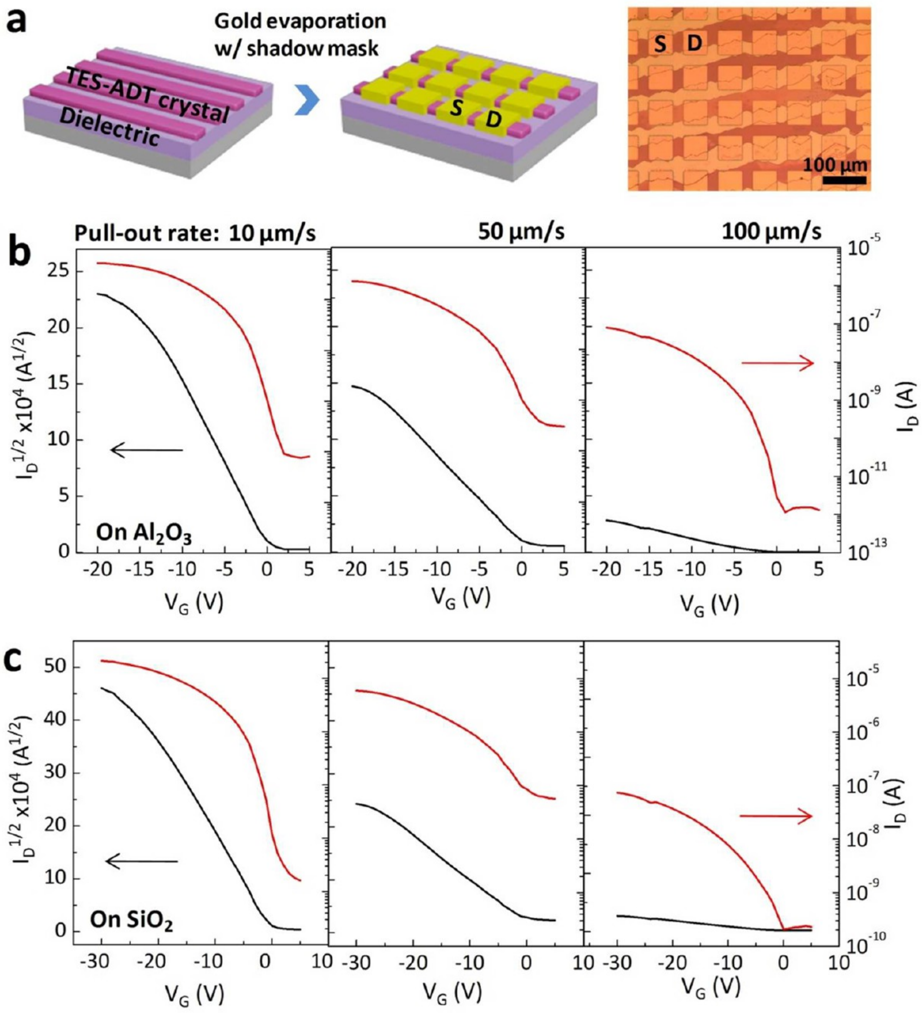

Figure 4. (a) Schematic illustrations of the fabrication process and device structures of the OFETs, and an OM image of a typical OFET batch of TES-ADT crystals produced at 10 μm/s. Typical transfer characteristics for the dip-coated TES-ADT-based OFETs using (b) Al_2O_3 dielectrics and (c) SiO_2 dielectrics as a function of the pull-out rate.

at higher pull-out rates on both substrates. The average saturation mobilities were 0.56 cm^2/(V s) (highest: 0.83 cm^2/(V s)) on Al_2O_3, and 1.2 cm^2/(V s) (highest: 1.82 cm^2/(V s)) on SiO_2 substrates. It is noteworthy that these high performance crystals were achieved using a one-step dip-coating process without postannealing steps, such as solvent vapor annealing. The transistor parameters were extracted from a random selection of 18−32 devices (6−8 devices in each batch, 3−4 batches in total). OM images of typical OFET batches using TES-ADT crystals grown at a pull-out rate of 10 μm/s are shown in Figure 4a. Figure 5a and c summarizes the μ and threshold voltage (V_{Th}) values of the TES-ADT thin films as a function of the pull-out rate. As the pull-out rate decreased from 100 to 10 μm/s, the mobility values increased sharply, and the V_{Th} values approached zero. This trend in the electrical characteristics of the TES-ADT thin films was agreed well with the results of the morphological, optical, and crystallographic studies of the OM/POM, out-of-plane mode XRD, AFM, and 2D-GIXD. The excellent μ and near-zero V_{Th} values of the crystals grown at 10 μm/s achieved without dielectric surface passivation verified their intrinsic highly crystalline qualities.[27,32] Crystals grown at 10 μm/s also exhibited good I_D versus drain voltage (V_D) output characteristics on both Al_2O_3 and SiO_2 dielectrics, as shown in Figure 5b and 5d, respectively.

Relationship between the Optimal Pull-Out Rate and the Self-Assembly of Soluble Acenes. In a previous study, we showed that optimized TIPS-PEN and FTES-ADT crystals could be grown at the same optimal pull-out rates (100−150 μm/s for dichloromethane solvent and 50 μm/s for chloroform solvent), depending on the solvent and solution temperature;[20] however, for TES-ADT, the optimal pull-out rate was 10 μm/s, which is different from the optimal rates for the TIPS-PEN or FTES-ADT (for the same solvent, dichloromethane). The difference between the optimal pull-out rates of TES-ADT and the other soluble acenes (TIPS-PEN and FTES-ADT) was investigated by examining the self-assembly of soluble acenes using in situ time-resolved confocal microscopy techniques. Solutions of TES-ADT, TIPS-PEN, and FTES-ADT in toluene (0.2 wt %) were prepared, and 10 μL droplets were dropped onto the cleaned Si wafers (see the schematic illustration shown in Figure 6a) (Here, we used toluene rather than dichloromethane for experimental ease because we could not observe the in situ crystallization behavior using dichloromethane due to its extremely low bp.). Figure 6a shows that the contact line of the TES-ADT droplet was not pinned, the diameter of the

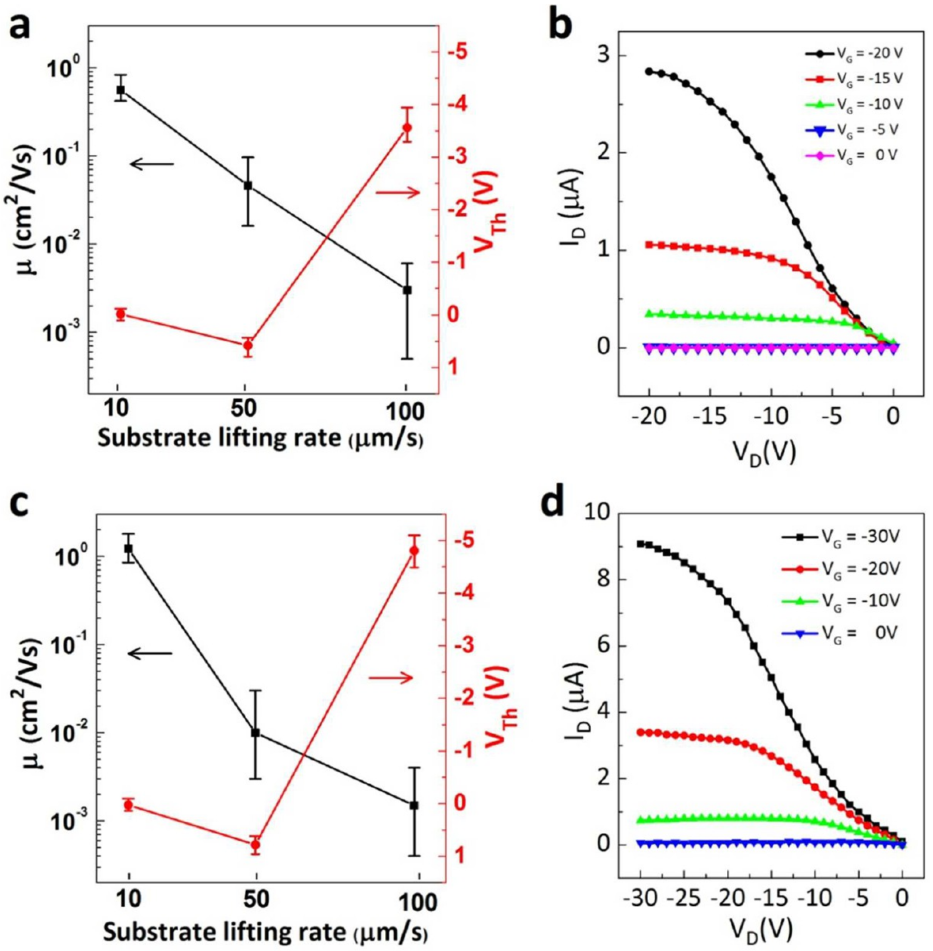

Figure 5. Summary of the transistor parameters of the dip-coated TES-ADT-based OFETs prepared using (a) Al_2O_3 dielectrics and (c) SiO_2 dielectrics as a function of the pull-out rate. Typical output characteristics of the dip-coated TES-ADT-based OFETs (for the TES-ADT crystal arrays grown at 10 μm/s) using (b) Al_2O_3 dielectrics and (d) SiO_2 dielectrics, respectively. C_i values of the Al_2O_3 and SiO_2 gate dielectrics are 64 and 32.4 nF/cm², respectively.

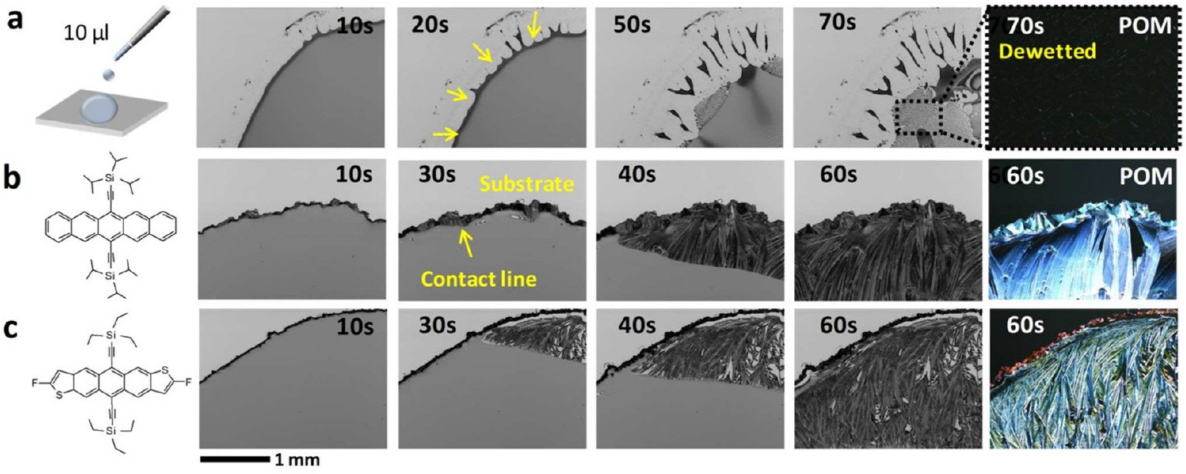

Figure 6. In situ time-resolved confocal microscopy images, OM, and POM images for 10 μL droplets of (a) TES-ADT, (b) TIPS-PEN, and (c) FTES-ADT solutions. (a inset) Illustration of the dropping experiment. (b and c) Chemical structures of TIPS-PEN and FTES-ADT, respectively.

droplet continuously decreased, and the TES-ADT molecules dewetted after the solvent had completely evaporated. The OM and POM images of the TES-ADT film (70 s after dropping) clearly showed that the dewetted TES-ADT morphology did not include any crystals. On the other hands, TIPS-PEN and FTES-ADT crystals initiated growth at the periphery and grew toward the center of a droplet (see Figure 6b and c, respectively). When the contact line was pinned during solvent drying, the difference between the solvent evaporation rates at the pinned contact line and at the center of the droplet

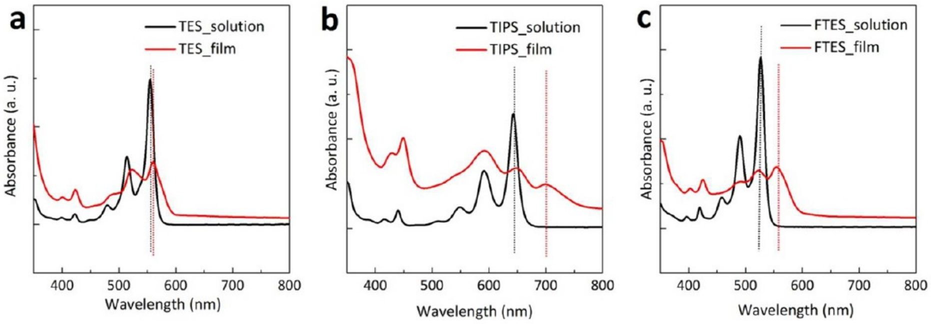

Figure 7. UV–vis absorption spectra of the dried droplets and the solutions for (a) TES-ADT, (b) TIPS-PEN, and (c) FTES-ADT.

imposed a concentration gradient between the regions.[33] As a result, if the concentration at the contact line reached a critical value for nucleation, TIPS-PEN or FTES-ADT crystals crystallized from the nucleation sites at the contact line.[34] Because the TIPS-PEN or FTES-ADT molecules were supplied from the center to the contact line via a concentration difference-induced hydrodynamic flow, the crystals grew from the contact line toward the internal region owing to strong intermolecular π-stacking.[33,34] Nucleation did not occur at the contact line of the TES-ADT film, indicating that the concentration critical for nucleation was higher and, therefore, the self-assembly was weaker than for TIPS-PEN or FTES-ADT. The same trend was observed by OM and POM for the final dried droplets of the soluble acene solutions with dichloromethane solvent (see the resulting OM and POM images in Supporting Information Figure S3) although we could not observe the in situ crystallization behavior due to its extremely low bp.

The crystallization behavior was further studied by comparing the UV–vis absorption spectra of three of the dried droplets with their solution-state samples. As shown in Figure 7a, the UV–vis spectra of the dried TES-ADT droplet showed a negligible red shift, or displacement (Δ), compared to the spectra of the solution-state samples. By contrast, the spectra of the TIPS-PEN (Figure 7b) or FTES-ADT (Figure 7c) samples showed a distinct red shift. The values of Δ were 5 nm or 161 cm^{-1} (in TES-ADT), 54 nm or 1194 cm^{-1} (in TIPS-PEN), and 31 nm or 1062 cm^{-1} (in FTES-ADT), respectively (see the Supporting Information for the calculation procedures). Because Δ resulted from the enhanced Coulombic interactions among the molecules in the thin film state compared to the solution state, a large value of Δ indicated an increasing the π–π stacking interactions among the acene backbones.[35,36] These results clearly showed that the TES-ADT molecules in the dried droplet were not sufficiently self-assembled, whereas the TIPS-PEN or FTES-ADT molecules formed highly crystalline nanostructures through their strong intermolecular interactions. In-situ time-resolved confocal microscopy and UV–vis studies indicated that the self-assembly of TES-ADT molecules was weaker than the self-assembly of TIPS-PEN or FTES-ADT.

Crystallization of organic semiconductors during dip-coating is an evaporation-induced process that occurs at the contact line.[7,37,38] The solution crystallization at the contact line is influenced by the evaporation rate of the solvent, the pull-out rate of the substrate, the rate of evaporation-induced convective flow, and the rate of self-assembly among solute molecules at the contact line.[23,37,38] Considering that the experimental dip-coating conditions were nearly identical (e.g., the pull-out rate, solution temperature, type of solvent, and substrate) for TES-ADT, TIPS-PEN, and FTES-ADT, we hypothesize that the self-assembly rate of the solute molecules was critical for determining the optimal pull-out rates. For this reason, the optimal pull-out rates of TES-ADT and TIPS-PEN/FTES-ADT differed. Our hypothesis was supported by the results of a concentration-dependent TES-ADT crystallization experiment conducted by dip-coating at a pull-out rate of 10 μm/s using dichloromethane as the solvent (see the resulting OM and POM images in the Supporting Information Figure S4). TES-ADT molecules did not crystallize at all from a 0.2 wt % solution, and they only crystallized into continuous arrays at higher solution concentrations of 0.7 wt %. The TIPS-PEN or FTES-ADT films formed highly crystalline arrays from 0.2 wt % solutions.[20] Because the concentration near the contact line was low and the evaporation-induced convective flow toward the contact line was weak at low concentrations, a 0.2 wt % solution was not sufficiently concentrated to support TES-ADT nucleation and crystallization.[39]

These considerations indicated that the weak tendency of TES-ADT to self-assembly, relative to the tendencies of TIPS-PEN or FTES-ADT, was associated with the reduced pull-out rate (10 μm/s) necessary to prepare optimized crystal arrays of TES-ADT. The pull-out rates that yielded optimized TIPS-PEN or FTES-ADT crystal arrays were 100–150 μm/s (dip-coating using dichloromethane). The lower pull-out rates allowed more solute molecules to migrate into the meniscus under the convective flow, thereby inducing the nucleation of the TES-ADT molecules.[40] Once the nucleation had initiated, the TES-ADT crystals grew directionally during dip-coating with a very low growth rate (the same rate as the pull-out rate: 10 μm/s). We believe that crystallization of TES-ADT into continuous stripes at 10 μm/s resulted from the initial nucleation stage at the initial contact line. Therefore, the regularity in initial nucleation sites of the dip-coated soluble acenes might be due to the fingering instability of the air–solution–substrate contact line.[41−43] In other words, the continuous line of TES-ADT at the air–solution–substrate contact line segregates into more concentrated, periodically distributed domains of TES-ADT due to the fingering instability of the drying front. When these periodically distributed domains are sufficiently concentrated to support nucleation, the regularly nucleated soluble acenes crystallized into continuous stripes as dip-coating proceeds, resulting in well-ordered crystal arrays. Since we used a quickly evaporating solvent, the contact line was not strongly pinned to the substrate and therefore it did not show so-called "slip-stick" behavior during dip-coating.[37]

This optimized dip-coating process was used to prepare highly crystalline aligned TES-ADT crystal arrays exhibiting excellent field-effect mobility values (up to 1.8 $\text{cm}^2/(\text{V s})$) without the need for solvent vapor annealing postprocessing. Because the dip-coating pull-out rate may be quantitatively controlled with a fine resolution (1 μm/s), dip-coating presents a systematic method for optimizing the crystallization of soluble acenes having a range of crystallization tendencies.

■ CONCLUSION

In conclusion, we report the preparation of high-performance TES-ADT-based OFETs without the need for solvent vapor annealing postprocessing, which was previously thought to be an essential step for improving the performances of TES-ADT-based OFETs. Highly crystalline TES-ADT crystal arrays were achieved via an one-step dip-coating process with an optimal pull-out rate of 10 μm/s, as confirmed by optical, crystallographic, morphological, and electrical analyses. The optimal pull-out rate was compared with the optimal rates of TIPS-PEN or FTES-ADT to identify a correlation between the optimal pull-out rate and the self-assembly tendency of the soluble acenes. Weak self-assembly tendencies yielded lower optimal pull-out rates. This conclusion was supported by the in situ observation of crystallization behavior using UV−vis spectroscopy and variable-concentration dip-coating experiments involving the soluble acenes. This study involved developing a facile one-step preparation of highly crystalline TES-ADT crystals, thereby demonstrating that the dip-coating technique presents a promising approach to optimizing the formation of thin films from a variety of soluble acenes having different self-assembly properties.

■ ASSOCIATED CONTENT

Ⓢ Supporting Information

Variable film morphologies of the TES-ADT thin films produced at a pull-out rate of 50 μm/s, schematic illustration of 2D-GIXD studies of the dip-coated TES-ADT thin films, optical images of the dried droplets of soluble acenes using dichloromethane solvent, and concentration-dependent crystallization of TES-ADT films. This material is available free of charge via the Internet at http://pubs.acs.org/.

■ AUTHOR INFORMATION

Corresponding Author

*E-mail: cep@postech.ac.kr (C.E.P.); jongjin00.park@samsung.com (J.-J.P.) Tel.: +82-54-279-2269. Fax: +82-54-279-8298.

Author Contributions

$^\nabla$These authors contributed equally.

Notes

The authors declare no competing financial interest.

■ ACKNOWLEDGMENTS

This work was supported by a grant from the Korea Science and Engineering Foundation (KOSEF), funded by the Korea government (MEST) (2012-0000127), and by the PAL, XFEL projects, Korea.

■ REFERENCES

(1) Dimitrakopoulos, C. D.; Malenfant, P. R. L. *Adv. Mater.* **2002**, *14*, 99−117.

(2) Braga, D.; Horowitz, G. *Adv. Mater.* **2009**, *21*, 1473−1486.

(3) Gundlach, D. J.; Royer, J. E.; Park, S. K.; Subramanian, S.; Jurchescu, O. D.; Hamadani, B. H.; Moad, A. J.; Kline, R. J.; Teague, L. C.; Kirillov, O.; Richter, C. A.; Kushmerick, J. G.; Richter, L. J.; Parkin, S. R.; Jackson, T. N.; Anthony, J. E. *Nat. Mater.* **2008**, *7*, 216−221.

(4) Park, S. K.; Mourey, D. A.; Subramanian, S.; Anthony, J. E.; Jackson, T. N. *Appl. Phys. Lett.* **2008**, *93*, 043301.

(5) Kim, S. H.; Choi, D.; Chung, D. S.; Yang, C.; Jang, J.; Park, C. E.; Park, S. −H. K. *Appl. Phys. Lett.* **2008**, *93*, 113306.

(6) Lim, J. A.; Lee, W. H.; Lee, H. S.; Lee, J. H.; Park, Y. D.; Cho, K. *Adv. Funct. Mater.* **2008**, *18*, 229−234.

(7) Sele, C. W.; Kjellander, B. K. C.; Niesen, B.; Thornton, M. J.; van der Putten, J. B. P. H.; Myny, K.; Wondergem, H. J.; Moser, A.; Resel, R.; van Breemen, A. J. J. M.; van Aerle, N.; Heremans, P.; Anthony, J. E.; Gelinck, G. H. *Adv. Mater.* **2009**, *21*, 4926−7931.

(8) Park, S. K.; Jackson, T. N.; Anthony, J. E.; Mourey, D. A. *Appl. Phys. Lett.* **2007**, *91*, 063514.

(9) Kim, Y.-H.; Lee, Y. U.; Han, J.-I.; Han, S.-M.; Han, M.-K. *J. Electrochem. Soc.* **2007**, *154*, H995−H998.

(10) Park, K.; Park, S. H.; Kim, E.; Kim, J.-D.; An, S.-Y.; Lim, H. S.; Lee, H. H.; Kim, D. H.; Ryu, D. Y.; Lee, D. R.; Cho, J. H. *Chem. Mater.* **2010**, *22*, 5377−5382.

(11) Pisula, W.; Menon, A.; Stepputat, M.; Lieberwirth, I.; Kolb, U.; Tracz, A.; Sirringhaus, H.; Pakula, T.; Müllen, K. *Adv. Mater.* **2005**, *17*, 684−689.

(12) Virkar, A. A.; Mannsfeld, S.; Bao, Z.; Stingelin, N. *Adv. Mater.* **2010**, *22*, 3857−3875.

(13) Nam, S.; Jang, J.; Cha, H.; Hwang, J.; An, T. K.; Park, S.; Park, C. E. *J. Mater. Chem.* **2012**, *22*, 5543−5549.

(14) Dickey, K. C.; Anthony, J. E.; Loo, Y.-L. *Adv. Mater.* **2006**, *18*, 1721−1726.

(15) Lee, S. S.; Kim, C. S.; Gomez, E. D.; Purushothaman, B.; Toney, M. F.; Wang, C.; Hexemer, A.; Anthony, J. E.; Loo, Y. −L. *Adv. Mater.* **2009**, *21*, 3605−3609.

(16) Lee, W. H.; Kim, D. H.; Cho, J. H.; Jang, Y.; Lim, J. A.; Kwak, D.; Cho, K. *Appl. Phys. Lett.* **2007**, *91*, 092105.

(17) Yu, L.; Li, X.; Pavlica, E.; Loth, M. A.; Anthony, J. E.; Bratina, G.; Kjellander, C.; Gelinck, G.; Stingelin, N. *Appl. Phys. Lett.* **2011**, *99*, 263304.

(18) Kim, S. H.; Hong, K.; Jang, M.; Jang, J.; Anthony, J. E.; Yang, H.; Park, C. E. *Adv. Mater.* **2010**, *22*, 4809−4813.

(19) Kim, S. H.; Jang, M.; Yang, H.; Anthony, J. E.; Park, C. E. *Adv. Funct. Mater.* **2011**, *21*, 2198−2207.

(20) Jang, J.; Nam, S.; Im, K.; Hur, J.; Cha, S. N.; Kim, J.; Son, H. B.; Suh, H.; Loth, M. A.; Anthony, J. E.; Park, J. −J.; Park, C. E.; Kim, J. M.; Kim, K. *Adv. Funct. Mater.* **2012**, *22*, 1005−1014.

(21) Becerril, H. A.; Roberts, M. E.; Liu, Z.; Locklin, J.; Bao, Z. *Adv. Mater.* **2008**, *20*, 2588−2594.

(22) Duffy, C. M.; Andreasen, J. W.; Breiby, D. W.; Nielsen, M. M.; Ando, M.; Minakata, T.; Sirringhaus, H. *Chem. Mater.* **2008**, *20*, 7252−7259.

(23) Payne, M. M.; Parkin, S. R.; Anthony, J. E.; Kuo, C. −C.; Jackson, T. N. *J. Am. Chem. Soc.* **2005**, *127*, 4986−4987.

(24) Fallahazad, B.; Lee, K.; Lian, G.; Kim, S.; Corbet, C. M.; Ferrer, D. A.; Colombo, L.; Tutuc, E. *Appl. Phys. Lett.* **2012**, *100*, 093112.

(25) Kim, J. B.; Fuentes-Hernandez, C.; Potscavage, W. J.; Zhang, X.-H., Jr.; Kippelen, B. *Appl. Phys. Lett.* **2009**, *94*, 142107.

(26) Jang, J.; Nam, S.; Yun, W. M.; Yang, C.; Hwang, J.; An, T. K.; Chung, D. S.; Park, C. E. *J. Mater. Chem.* **2011**, *21*, 12542−12546.

(27) Rivnay, J.; Jimison, L. H.; Northrup, J. E.; Toney, M. F.; Noriega, R.; Lu, S.; Marks, T. J.; Facchetti, A.; Salleo, A. *Nat. Mater.* **2009**, *8*, 952−958.

(28) Li, L.; Schuermann, K. C.; Ostendorp, S.; Wang, W.; Du, C.; Lei, Y.; Fuchs, H.; de Cola, L.; Müllen, K.; Chi, L. *J. Am. Chem. Soc.* **2010**, *132*, 8807−8809.

(29) Cheng, H. −L.; Mai, Y. −S.; Chou, W. −Y.; Chang, L. −R.; Liang, X. −W. *Adv. Func. Mater.* **2007**, *17*, 3639−3649.

(30) Gundlach, D. J.; Lin, Y. Y.; Jackson, T. N.; Nelson, S. F.; Schlom, D. G. *IEEE Electron Device Lett.* **1997**, *18*, 87−89.

(31) Lee, W. H.; Lim, J. A.; Kwak, D.; Cho, J. H.; Lee, H. S.; Choi, H. H.; Cho, K. *Adv. Mater.* **2009**, *21*, 4243−4248.
(32) Pernstich, K. P.; Haas, S.; Oberhoff, D.; Goldmann, C.; Gundlach, D. J.; Batlogg, B.; Rashid, A. N.; Schitter, G. *J. Appl. Phys.* **2004**, *96*, 6431−6438.
(33) Deegan, R. D.; Bakajin, O.; Dupont, T. F.; Huber, G.; Nagel, S. R.; Witten, T. A. *Nature* **1997**, *389*, 827−829.
(34) Lim, J. A.; Lee, W. H.; Kwak, D.; Cho, K. *Langmuir* **2009**, *25*, 5404−5410.
(35) Platt, A. D.; Day, J.; Subramanian, S.; Anthony, J. E.; Ostroverkhova, O. *J. Phys. Chem. C* **2009**, *113*, 14006−14014.
(36) Ostroverkhova, O.; Shcherbyna, S.; Cooke, D. G.; Egerton, R. F.; Hegmann, F. A.; Tykwinski, R. R; Parkin, S. R.; Anthony, J. E. *J. Apply. Phys.* **2005**, *98*, 033701.
(37) Zhang, C.; Zhang, X.; Zhang, X.; Fan, X.; Jie, J.; Chang, J. C.; Lee, C. −S.; Zhang, W.; Lee, S. −T. *Adv. Mater.* **2008**, *20*, 1716−1720.
(38) Huang, J.; Fan, R.; Connor, S.; Yang, P. *Angew. Chem., Int. Ed.* **2007**, *46*, 2414−2417.
(39) Liu, N.; Zhou, Y.; Wang, L.; Peng, J.; Wang, J.; Pei, J.; Cao, Y. *Langmuir* **2009**, *25*, 665−671.
(40) Jung, B. G.; Min, S.-H.; Kwon, C.-W.; Park, S.-H.; Kim, K.-B.; Yoon, T.-S. *J. Electrochem. Soc.* **2009**, *156*, K86−K90.
(41) Huang, J.; Kim, F.; Tao, A. R.; Connor, S.; Yang, P. *Nat. Mater.* **2005**, *4*, 896.
(42) Cazabat, A. M.; Heslot, F.; Troian, S. M.; Carles, P. *Nature* **1990**, *346*, 824.
(43) Fitzgerald, S. D.; Woods, A. W. *Nature* **1994**, *367*, 450.